photonics

MDPI

Communication

Diode-End-Pumped Continuous-Wave Tunable Nd^{3+}:$LiYF_4$ Laser Operating on the $^4F_{3/2} \rightarrow {}^4I_{13/2}$ Transition

Chu Chu [1,*], Shuang Wang [2], Xinhua Fu [3] and Zhenhua Du [4,*]

[1] School of Physics and Optoelectronic Engineering, Harbin Engineering University, Harbin 150001, China
[2] School of Physics, Changchun University of Science and Technology, Changchun 130022, China; wangshuangcust@163.com
[3] School of Opto-Electronics Engineering, Changchun University of Science and Technology, Changchun 130022, China; fuxinhua1976@163.com
[4] School of Physical Science and Technology, Bohai University, Jinzhou 121013, China
* Correspondence: cccchuchu1997@163.com (C.C.); duzh1992@163.com (Z.D.)

Abstract: A laser diode (LD) end-pumped continuous-wave (CW) tunable Nd^{3+}:$LiYF_4$ (Nd:YLF) laser operating on the $^4F_{3/2} \rightarrow {}^4I_{13/2}$ transition was performed. Four single-wavelength (SW) lasing at 1321, 1314, 1371, and 1364 nm in the π-polarized direction and three SW lasing at 1314, 1326, and 1371 nm in the σ-polarized direction were achieved using a tuning prism. At 20 W pump power, the σ-polarized 1314 nm emission generated 7.3 W power output with 39.4% slope efficiency. Further, the three-pair of switchable π-polarized dual-wavelengths (DWs) at 1321/1314 nm, 1371/1364 nm, and 1321/1364 nm and the two-pair of switchable σ-polarized DWs at 1314/1326 nm and 1314/1371 nm were also realized by rotating an intracavity birefringence filter (BF). In addition, by employing dual intracavity BFs, the balanced DW output power was attained, achieving 6.4 W total maximum output at 1314/1321 nm in the π-polarized direction.

Keywords: solid-state laser; tunable laser; Nd^{3+}:$LiYF_4$; birefringence filter

check for updates

Received: 23 May 2025
Revised: 11 June 2025
Accepted: 13 June 2025
Published: 14 June 2025

Citation: Chu, C.; Wang, S.; Fu, X.; Du, Z. Diode-End-Pumped Continuous-Wave Tunable Nd^{3+}:$LiYF_4$ Laser Operating on the $^4F_{3/2} \rightarrow {}^4I_{13/2}$ Transition. *Photonics* **2025**, *12*, 613. https://doi.org/10.3390/photonics12060613

Copyright: © 2025 by the authors. Licensee MDPI, Basel, Switzerland. This article is an open access article distributed under the terms and conditions of the Creative Commons Attribution (CC BY) license (https://creativecommons.org/licenses/by/4.0/).

1. Introduction

Continuous-wave (CW) lasers emitting in the 1.3–1.4 μm spectral range have gained significant attention due to their diverse applications, including medical laser technologies, environmental monitoring, fiber-optic telecommunications, and visible light generation through nonlinear optical processes [1–5]. Recent advancements in solid-state laser systems have demonstrated successful implementation of single-wavelength (SW) operation within this spectral band using various Nd-doped laser crystals. Notable achievements include development in Nd:YAG [6,7], Nd:Vanadates [7–15], Nd:YLF [16], and Nd:YAP [17], highlighting progress in this technologically important wavelength region. Dual-wavelength (DW) lasers with the orthogonal polarization demonstrate significant potential across multiple technological domains, particularly in advanced optical applications such as atmospheric sensing [18], biomedical device development [19], holographic imaging [20,21] and ultra-precise spectral analysis [22]. Their unique wavelength combination capability enables critical functions in self-referencing metrological systems [23], visible/UV light generation via sum-frequency generation and THz wave production via difference-frequency generation [24–28]. In parallel, DW lasers with the same polarization enhance precision metrology and lidar systems by minimizing phase noise and improving interference stability, crucial for atmospheric sensing and high-resolution distance measurements [29]. Additionally, identical polarization alignment in fiber-optic communication (such as wavelength division multiplexing) suppresses inter-channel crosstalk, enabling higher data

transmission capacity [30]. Of particular scientific interest are DWs within the 1.3–1.4 μm spectral band [31–35], which show exceptional applicability in quantum precision instruments like silver atom optical clocks, atomic cooling systems operating beyond Doppler limitations, and advanced phototherapeutic implementations [36–38]. As a prominent active medium for solid-state laser systems, Nd:YLF crystals exhibit distinctive advantages including intrinsic birefringent properties, minimized thermal lensing effects, and extended radiative decay characteristics [39–43]. Figure 1 illustrates the wavelength-dependent emission cross-sections across the 1.3–1.4 μm spectral range, derived through calculation using the Füchtbauer–Ladenburg formalism [44]. In this study, we achieved the first tunable SW and DW lasers in Nd:YLF crystal in the 1.3–1.4 μm spectral region. Seven CW SWs are realized with the tuning prism. Further, the five-pair of CW DWs are obtained with an intracavity birefringence filter (BF). In addition, the balanced DW power output was also generated with the dual intracavity BFs.

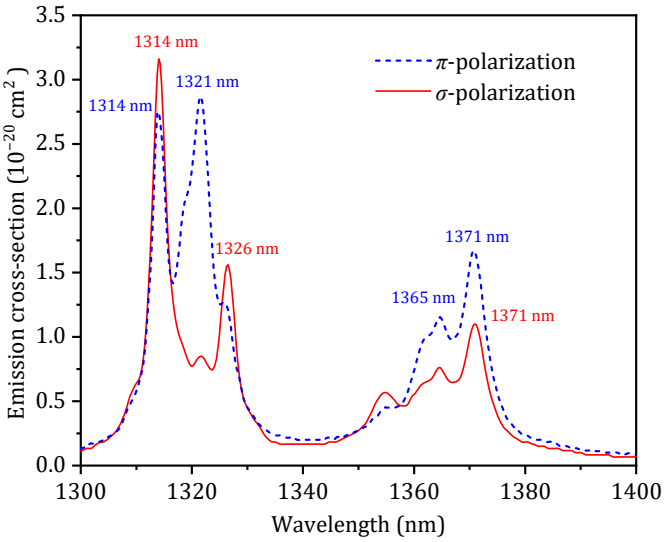

Figure 1. Emission spectra of the Nd:YLF in the 1.3–1.4 μm spectral region.

2. Experimental Details

The schematic diagram of the tunable Nd:YLF laser operating on the $^4F_{3/2} \rightarrow {}^4I_{13/2}$ transition is displayed in Figure 2a. The pumping source was an LD, providing a central emission wavelength at 806 nm and a 20 W maximum power. The pump light was output by an optical fiber coupling with a 400 μm core diameter and a 0.22 numerical aperture. The spot radius of the pump light was 200 μm. Both identical convex lenses (L_1 and L_2) with a focal length of the 150 mm and anti-reflection (AR) film for the pump wavelength was used to collimate and focus the pump light into the active medium. A Nd:YLF cut along the *a*-axis (1.0 at.% doping, 5 mm length) functioned as the active medium with AR at 806 nm and 1310–1380 nm, which was sealed in indium foil and affixed to red copper mounts equipped with water cooling, maintained at 15 °C. The cavity input coupler was a planar mirror (M_1) with high reflectivity (HR) for 1310–1380 nm and AR for 806 nm, 1040–1060 nm. The cavity output coupler was a concave mirror (M_2) of −300 mm radius of curvature with a transmittance (T_{oc}) of 3.5% at 1310–1380 nm. Two other couplers (T_{oc} = 2.0% and T_{oc} = 5.0%) were also carried out, with the M_2 demonstrating the optimal output performance. To obtain SW tuning, a prism with AR for 1310–1380 nm and a plane reflector (M_3) with HR for 1310–1380 nm were utilized. By adjusting the M_3, SW tuning can be achieved. A polarization beam splitter (PBS) was used to separate two laser beams with orthogonal polarization. To realize DW tuning, a 1.0 mm-thick quartz BF_1 was employed

as a tuning element, as displayed in Figure 2b. To obtain the balanced DW power output, both BF_1 and BF_2 (0.5 mm thick) were utilized, as displayed in Figure 2c. To realize the π-polarized DW laser, the placement direction of BF_1 is displayed in Figure 2d. The BF_1 placed in this way can effectively suppress the σ-polarization because when the direction of the σ-polarized beam was perpendicular to the incident plane (S-wave), the reflection loss of the S-wave was the greatest when it was incident at the Brewster angle. Similarly, the placement direction of BF_2 can suppress the π-polarized beam and achieve σ-polarized DW laser output.

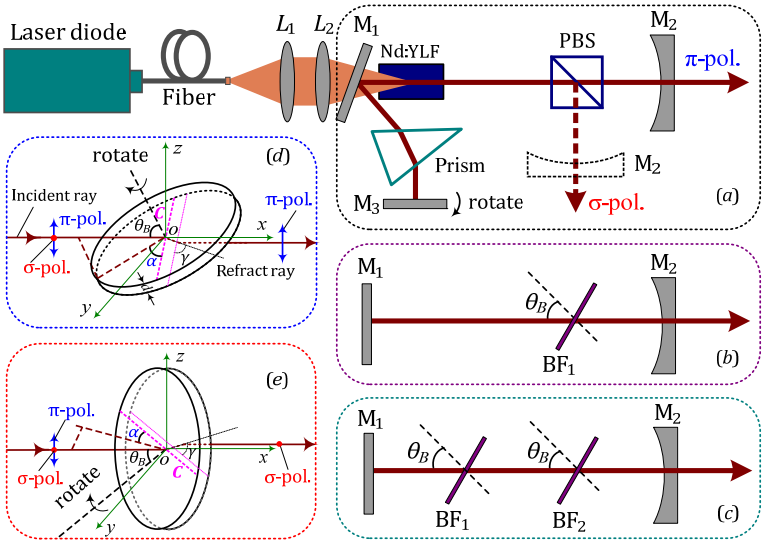

Figure 2. The schematic diagrams for SW (**a**), DW (**b**) and balanced power DW (**c**) tunable Nd:YLF laser. (**d**,**e**) are the BF_1 and BF_2 with orthogonal incident planes, respectively. θ_B is the Brewster angle, *C* is the crystal axis of the quartz BF_1 and BF_2.

3. Results and Discussion

The wavelength tuning was achieved by rotating the reflector M_3, enabling discrete π-polarized lasing at 1321, 1314, 1371, and 1364 nm wavelengths, as detailed in Figure 3. Under 20 W pumping, the laser demonstrated output powers reaching 6.71 (1321 nm), 6.02 (1314 nm), 4.11 (1371 nm), and 1.80 (1364 nm) with corresponding lasing thresholds of 1.52, 1.61, 2.70, and 4.22 W, respectively. Their corresponding slope/optical efficiencies were 36.1/33.5% (1321 nm), 33.2/30.0% (1314 nm), 23.9/20.5% (1371 nm), and 11.6/9.0% (1364 nm), respectively. In a four-level laser system, the emission cross-section of the laser transition wavelength is a key influencing factor of the output power. The size of the emission cross-section of the transition wavelength in Figure 1 is consistent with the trend of the output power obtained experimentally. Using the LABRAM-UV spectrum analyzer (HORIBA France SAS, Paris, France) with a resolution of 0.01 nm to scan the laser wavelengths and deal with the data with software, the laser spectra of the π-polarized SW emissions at the maximum pumping, as displayed in Figure 4. The central wavelengths were 1321.2, 1314.0, 1370.6, and 1364.4 nm with the corresponding linewidths (FWHM) of 0.20, 0.16, 0.18, and 0.22 nm. Their corresponding beam quality factors (M^2) were 1.11, 1.08, 1.20, and 1.14, respectively. The power stabilities of the SW lasers were measured with a precision power meter, demonstrating all <2.3% over a 1 h.

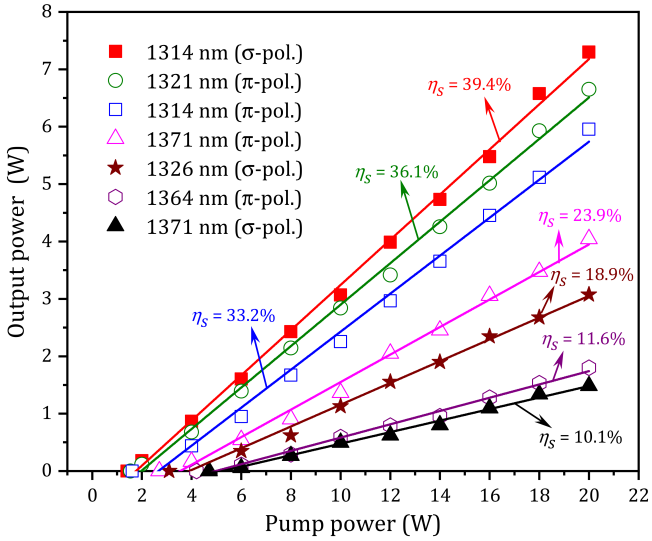

Figure 3. Output power of the SWs versus the pump power of 806 nm.

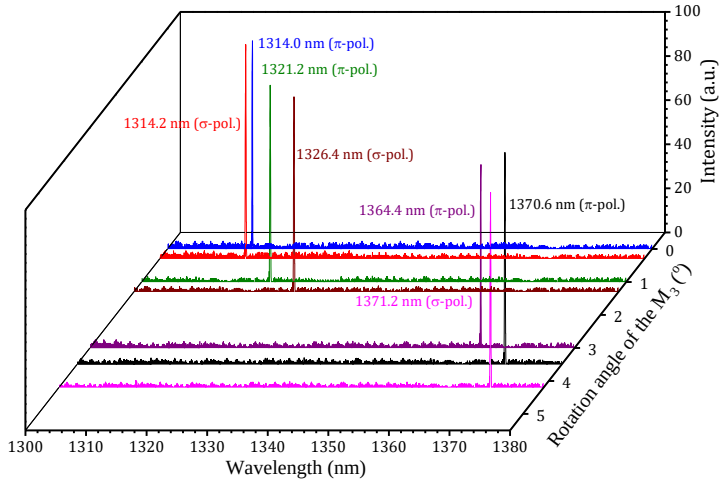

Figure 4. Output spectra of the SWs for the Nd:YLF laser operating on the $^4F_{3/2} \rightarrow {}^4I_{13/2}$ transition.

Similarly, the three σ-polarized SWs (1314.2, 1326.4, and 1371.2 nm) were also generated, as detailed in Figure 3. Under 20 W pumping, the laser demonstrated output powers reaching 7.30 (1314 nm), 3.09 (1326.4 nm), and 1.51 W (1371.2 nm), with corresponding lasing thresholds measured at 1.40, 3.11, and 4.72 W, respectively. Their slope/optical conversion efficiencies reached 39.4/36.5% (1314.2 nm), 18.9/16.5% (1326.4 nm), and 10.1/7.5% (1371.2 nm), respectively. The laser spectra of the σ-polarized SW emissions at the maximum pumping are also displayed in Figure 4. The linewidths of 1314.2, 1326.4, and 1371.2 nm were 0.15 (M^2 = 1.12), 0.19 (M^2 = 1.19) and 0.23 nm (M^2 = 1.23), respectively. The power stabilities of the three SW lasers were all <5% over 1 h.

The single-pass transmittance, T_{BF} (λ_i), for different lasing wavelengths, λ_i, transmitted through the BF is expressed as [45]

$$T_{BF,i} = 1 - 4\cot^2\gamma\tan^2\theta_B\left(1 - \cot^2\gamma\tan^2\theta_B\right)\sin^2\left(\frac{\delta_i}{2}\right), \quad (1)$$

where i represents different lasing wavelengths, γ is an angle between the incident ray and the BF crystal axis, α (tuning angle or rotation angle) is an angle between the crystal axis and the surface of the BF, θ_B is the Brewster angle, $\cos\gamma = \cos\theta_B\cos\alpha$, $\delta_i = 2\pi d\ (n_o - n_e)(1 - \cos^2\alpha\cos^2\theta_B)/\lambda_i\sin\theta_B$ is an optical phase difference, n_e and n_o are the refractive indices of *e*- and *o*-light, respectively, and d is the thickness of BF.

Using Equation (1) with the parameters: θ_B = 57.15°, n_e = 1.5534, n_o = 1.5443, and d = 1 mm, the cavity round-trip (dual-pass) transmittance ($T^2_{BF1,i}$) versus tuning angle (α) of the BF_1 are displayed in Figure 5. It could be observed in Figure 5 that $T^2_{BF,i}$ can be controlled by adjusting the BF_1. Thus, the lasing output can be tuned between the emission wavelengths. For a four-level laser system operating with CW, the oscillation threshold of each emission wavelength in a DW operation is given by [46]

$$P_{th,i} = \frac{-ln(1-T_{oc}) + L_i + L_{0i}}{2l_c\eta_{q,i}} \frac{h\nu_p}{\sigma_i\tau_i} \frac{1}{\iiint r_p(r,z)s_i(r,z)dv}, \quad (2)$$

where T_{oc} is the cavity mirror transmittance, $L_i = 1 - T^2_{BF1,i}$ is the cavity dual-pass loss, L_{0i} is the cavity dual-pass passive loss, $h\upsilon_p$ is the energy of a pump photon, l_c is the length of the active medium, $\eta_{q,i}$ is the quantum efficiency, τ_i is the radiation lifetime, σ_i is the emission cross-section, $r_p(r,z)$ is the distribution the pump beam for the normalized intensity in the Nd:YLF, and $s_i(r,z)$ is the cavity mode distribution of the normalized intensity for the emission wavelength. $r_p(r,z)$ and $s_i(r,z)$ can be expressed as follows [47], respectively,

$$r_p(r,z) = \frac{\alpha e^{-\alpha z}}{\pi\omega_p^2(z)(1-e^{-\alpha z})}\Theta\left[\omega_p^2(z) - r^2\right], \quad (3)$$

and

$$s_i(r,z) = \frac{2}{\pi\omega_i^2 l_c} e^{2r^2/\omega_i^2}, \quad (4)$$

where α (=5.0 cm^{-1}) is the absorption coefficient, r and z are radial and lateral coordinates, respectively, ω_i is the laser spot radius, Θ is the Heaviside step function, and pump beam size in the Nd:YLF crystal is given by

$$\omega_p^2(z) = \omega_{p0}^2\left\{1 + \left[\frac{\lambda_p M_p^2}{n\pi\omega_{p0}^2}(z - z_0)\right]^2\right\}, \quad (5)$$

where ω_{p0} is the pump spot radius, ω_i is the laser spot radius, λ_p is the pump wavelength, M_p^2 (=45) is the quality factor of pump beam, and z_0 is focal plane of the pump beam in the active medium. According to Equations (2)–(5), the π-polarized laser threshold power ($Pth_{,i}$) versus the tuning angle are displayed in Figure 6. It could be observed that the laser threshold power can be controlled by adjusting the BF_1. It could also be shown that there were crosspoints between any two of the three curves. When the pump power was controlled at a certain intersection point, DW laser could be generated simultaneously.

By controlling the tuning angle α, the three-pair of the π-polarized DW lasers at 1321/1314, 1371/1364, and 1364/1321 nm were attained, respectively. The DW laser was separated into the same polarized beams with a flexible wavelength selector Mono F-14 (Spectrolight Inc., Irvine, CA, USA), and the output power for individual wavelengths were measured respectively. The DW laser output–input powers are displayed in Figure 7. At 20 W pump power, the total CW output power of 7.01 (3.71/3.30 W at 1321/1314 nm), 3.12 (1.71/1.41 W at 1371/1364 nm), and 0.78 W (0.45/0.33 W at 1321/1364 nm) were attained, respectively. Their total corresponding optical conversion efficiencies reached 35.1, 16.5, and 3.9%, respectively. The π-polarized DW spectra at the maximum pumping are displayed in Figure 8. The central wavelengths were 1321.3/1314.1 nm, 1370.6/1364.4 nm, and 1321.2/1364.1 nm, with the spectral line widths of 0.23/0.17 nm, 0.14/0.17 nm, and 0.20/0.21 nm, respectively. The M^2 factors of the three-pair of DWs were all <1.26. The power stabilities of the three-pair of DWs were all <4.0%.

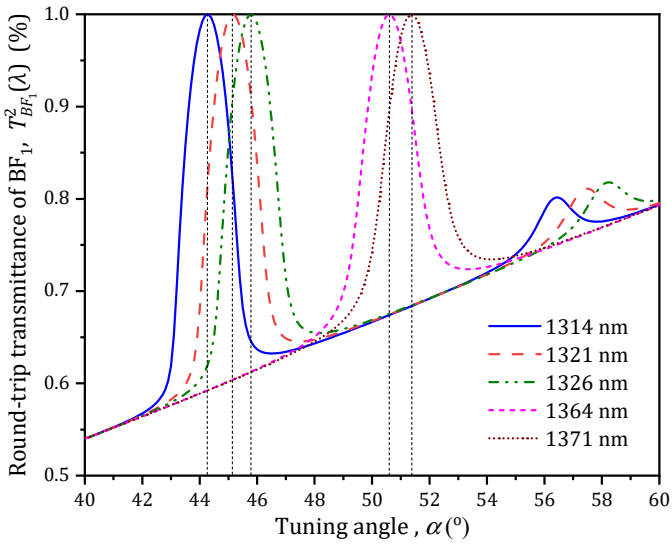

Figure 5. Round-trip (dual-pass) transmittance versus tuning angle of BF_1.

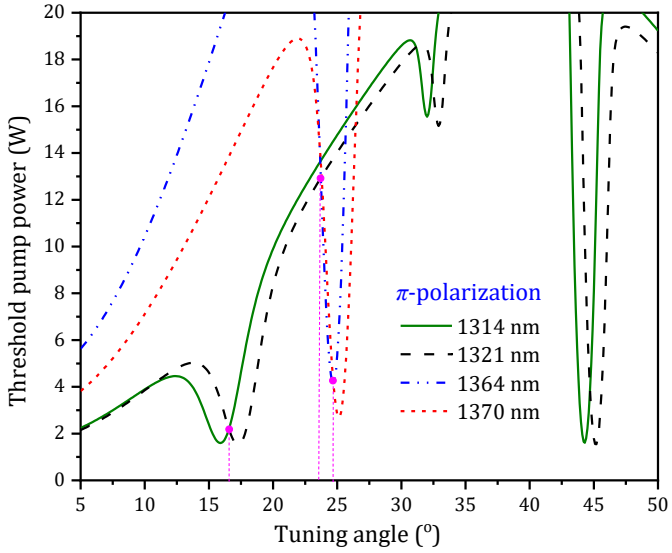

Figure 6. π-polarized threshold power of the DW laser versus the tuning angle of the BF_1.

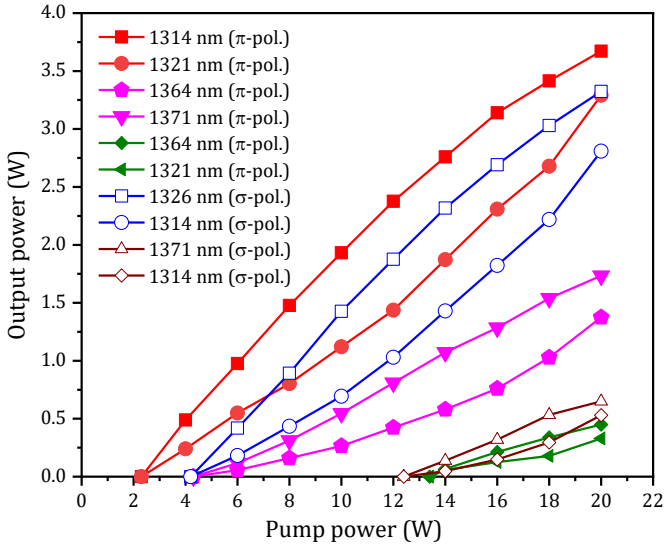

Figure 7. DW output power in the two polarized directions versus the pump power.

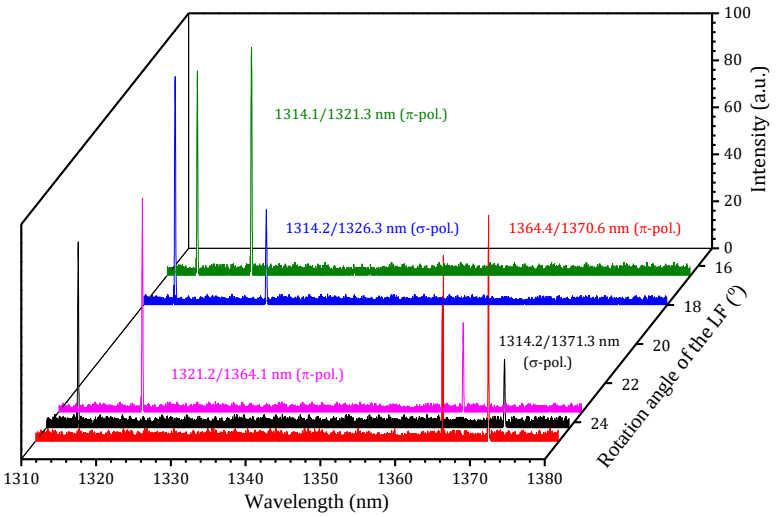

Figure 8. Output spectra of the DWs for the Nd:YLF laser operating on the $^4F_{3/2} \rightarrow {}^4I_{13/2}$ transition.

Similarly, the σ-polarized threshold power of the DW laser versus the tuning angle is displayed in Figure 9. The two-pair of σ-polarized DWs of 1326/1314 and 1371/1314 nm were realized. The power characteristics are displayed in Figure 7. The maximum total outputs of 6.10 (3.31/2.79 W at 1326/1314 nm) and 1.18 W (0.65/0.53 W at 1371/1314 nm) were attained, respectively. Their total corresponding optical efficiencies were 30.5, 16.5, and 5.9%, respectively. The σ-polarized DW spectra are also displayed in Figure 8. The central wavelengths were 1326.3/1314.2 nm and 1371.3/1314.2 nm, with spectral line widths of 0.15/0.17 nm and 0.17/0.20 nm, respectively. The M^2 factors of the two-pair of DWs were all <1.36. The power stabilities of the two-pair of DWs were all <4.5%.

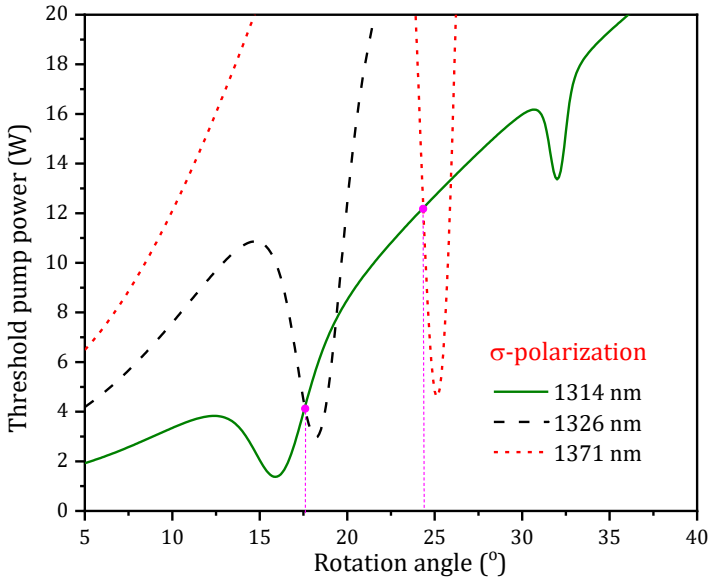

Figure 9. σ-polarized threshold power of the DW laser versus the tuning angle of the BF_1.

The slope efficiency of the input–output power for a four-level laser system can be given by [47]

$$\eta_{s,i} = \frac{-ln(1 - T_{oc})\eta_{q,i}}{-ln(1 - T_{oc})\eta_{q,i} + L_i + L_{0i}}. \quad (6)$$

Take the σ-polarized DW at 1326/1314 nm as an instance to demonstrate the achievement of a balanced output of the DW power. It can be obtained in Equation (2) that the

equal threshold power for 1326 nm and 1314 nm DW operation requires $L_{1326} < L_{1314}$. From Equation (3), it can be seen that $\eta_{s,1326} > \eta_{s,1314}$ when $L_{1326} < L_{1314}$ and $L_{0,1326} \approx L_{0,1314}$. A simple schematic is displayed in Figure 10a. This suggests that the two power outputs of the DW cannot be balanced. Hence, if the two output powers of the DW are to be balanced, a new intracavity loss must be introduced to break the DW equal threshold. A BF_2 was put in the resonator, the dual-pass transmittance ($T^2_{BF2,i}$) of 1326 nm and 1314 nm was calculated as a function of tuning angle (β), as displayed in Figure 10. When the tuning angle of the BF_1 was at α = 18° and the BF_2 was adjusted between 0–12°, $\eta_{s,1326} > \eta_{s,1314}$ was still maintained to be calculated by Equation (6), but $P_{th,1326} < P_{th,1314}$, as displayed in Figure 10b. This suggests that their slope efficiencies always had an intersection point, that was, equal power values could be found.

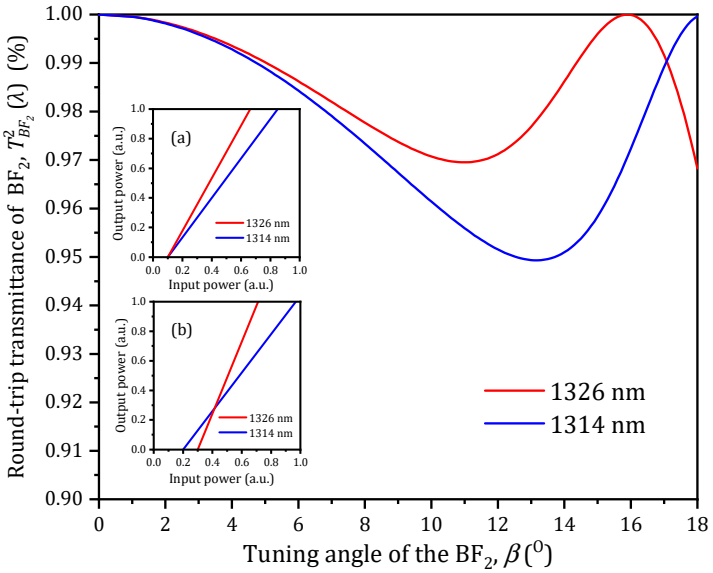

Figure 10. Dual-pass transmittance versus tuning angle of BF_2. (**a**) Slope efficiencies of 1326 and 1314 nm at $P_{th,1326} = P_{th,1314}$. (**b**) Slope efficiencies of 1326 and 1314 nm at $P_{th,1326} > P_{th,1314}$.

A balanced DW power at 1326/1314 nm in the σ-polarized direction was achieved with a total power output of 5.21 W at the maximum pumping by adjusting the BF_2. The output–input characteristic of the DW is displayed in Figure 11. The corresponding total slope/optical efficiency was 33.6/26.1%. The M^2 factor of the DW laser was <1.15. The power stability of the DW was <2.2% in 1 h. When the tuning angle of the BF_1 was at α = 24° and the BF_2 was adjusted, a balanced DW at 1314/1370 nm in the σ-direction was also achieved with a total power of 1.01 W, as also displayed in Figure 11. The corresponding total slope/optical efficiency was 13.2/5.1%. The M^2 factor of the DW laser was <1.20. The power stability of the DW was <3.6% in 1 h. The direction of the BF_1 and BF_2 was adjusted so that the direction of the incident plane of the light was rotated by 90 degrees, as displayed in Figure 2e. The three-pair of the balanced DW at 1314/1321, 1364/1371, and 1321/1364 nm were also generated, respectively. The output–input characteristics of the DWs are also displayed in Figure 11. The total power was 6.42 (1321/1314 nm), 2.61 (1371/1364 nm), and 0.62 W (1364/1321 nm), respectively. The M^2 factors of the DW lasers were <1.32. The power stabilities of the DW lasers were all <4.0% in 1 h.

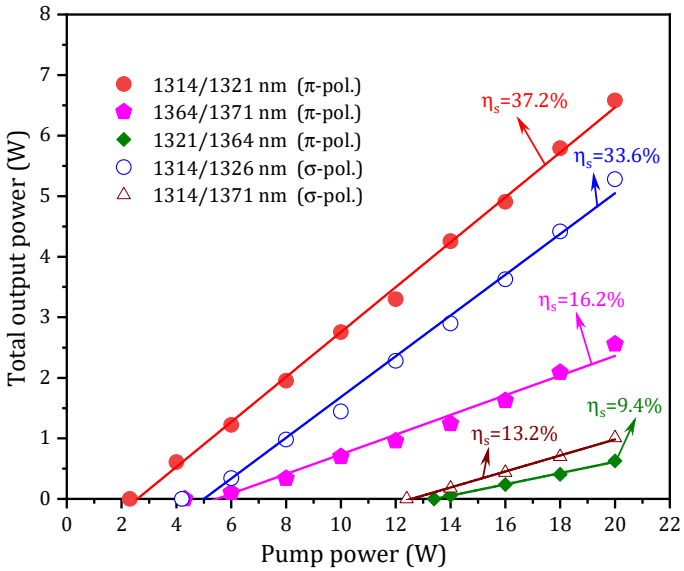

Figure 11. Total DW output power versus the pump power.

4. Conclusions

A LD-pumped CW tunable Nd:YLF laser operating on the $^4F_{3/2} \rightarrow {}^4I_{13/2}$ transition was demonstrated. Four π-polarized SW lasing at 1321, 1314, 1371, and 1364 nm and three σ-polarized SW lasing at 1314, 1326, and 1371 nm were achieved using a tuning prism. At 20 W pump power, the σ-polarized 1314 nm emission generated 7.3 W maximum power output with 39.4% slope efficiency. Further, the three-pair of switchable π-polarized DWs at 1321/1314 nm, 1371/1364 nm, and 1321/1364 nm and the two-pair of switchable σ-polarized DWs at 1314/1326 nm and 1314/1371 nm were also realized by rotating an intracavity BF. In addition, by employing dual intracavity BFs, the balanced DW output power was attained, achieving 6.4 W total maximum output at 1314/1321 nm in the π-polarized direction. We believe that the method presented in this paper has the potential to be extended to other laser crystals for obtaining tunable SW and DW lasers.

Author Contributions: Writing—original draft, C.C.; writing—review and editing, X.F.; investigation, S.W.; writing—review and editing, project administration, Z.D. All authors have read and agreed to the published version of the manuscript.

Funding: This work was supported by the Natural Science Training Project of Bohai University (0524xn04801, 0523bs05003).

Institutional Review Board Statement: Not applicable.

Informed Consent Statement: Informed consent was obtained from all subjects involved in this study.

Data Availability Statement: Data is contained within the article.

Conflicts of Interest: The authors declare no conflicts of interest.

References

1. Jaque, D.; Capmany, J.; Solé, J. Red, green, and, blue laser light from a single Nd:$YAl_3(BO_3)_4$ crystal based on laser oscillation at 1.3 μm. *Appl. Phys. Lett.* **1999**, *75*, 325–327. [CrossRef]
2. Chen, Y.; Liu, K.; He, L.; Yang, J.; Zong, N.; Yang, F.; Gao, H.; Liu, Z.; Yuan, L.; Lan, Y. 10 kHz ps 1342 nm laser generation by an electro-optically cavity-dumped modelocked Nd:YVO_4 laser. *Opt. Laser Technol.* **2017**, *87*, 26–30. [CrossRef]
3. Xu, B.; Wang, Y.; Lin, Z.; Peng, J.; Cheng, Y.; Luo, Z.; Xu, H.; Cai, Z.; Weng, J.; Moncorge, R. Single- and multi-wavelength Nd:$YALO_3$ lasers at 1328, 1339 and 1364 nm. *Opt. Laser Technol.* **2016**, *81*, 1–6. [CrossRef]
4. Cong, H.; Xue, C.; Zheng, J.; Yang, F.; Yu, K.; Liu, Z.; Zhang, X.; Cheng, B.; Wang, Q. Silicon based GeSn p-i-n photodetector for SWIR detection. *IEEE Photonics J.* **2016**, *8*, 6804706. [CrossRef]

5. Zhang, G.; Shen, H.; Zeng, R.; Huang, C.; Lin, W.; Huang, J. The study of 1341.4 nm Nd:$YAlO_3$ laser intracavity frequency-doubling by LiB_3O_5. *Opt. Commun.* **2000**, *183*, 461–466. [CrossRef]
6. Yue, S.; Cao, S.; Qin, W.; Jiang, M.; Liu, Y.; Cao, Y.; Wang, Z. Generation of 1319 nm Pulsed Vortex Laser by Annular Pumped Bonded Nd:YAG/V:YAG Crystal. *Photonics* **2025**, *12*, 303. [CrossRef]
7. Ma, F.; Wang, S.; Li, B.; Shang, P.; Li, J.; Li, Z. Effect of Lower-Level Relaxation on the Pulse Generation Performance of Q-Switched Nd:YAG Laser. *Photonics* **2025**, *12*, 408. [CrossRef]
8. Lenhardt, F.; Nittmann, M.; Bauer, T.; Bartschke, J.; Lhuillier, J. High-power 888-nm-pumped Nd:YVO_4 1342-nm oscillator operating in the TEM_{00} mode. *Appl. Phys. B* **2009**, *96*, 803. [CrossRef]
9. Li, F.; Liu, K.; Han, L.; Zong, N.; Bo, Y.; Zhang, J.; Peng, Q.; Cui, D.; Xu, Z. High-power 880-nm diode-directly-pumped passively mode-locked Nd:YVO_4 laser at 1342 nm with a semiconductor saturable absorber mirror. *Opt. Lett.* **2011**, *36*, 1485–1487. [CrossRef]
10. Jessica, D.; Luciana, R.; Wetter, N. Nd:YVO_4 Random Laser with Preferential Emission at 1340 nm over 1064 nm. *Photonics* **2024**, *11*, 898. [CrossRef]
11. Ogilvy, H.; Withford, M.; Dekker, P.; Piper, J. Efficient diode double-end-pumped Nd:YVO_4 laser operating at 1342 nm. *Opt. Express* **2003**, *11*, 2411–2415. [CrossRef] [PubMed]
12. Lü, Y.; Xia, J.; Wang, J.; Sun, G.; Zhang, X.; Zhang, A.; Yin, X.; Bao, L.; Quan, H. High-efficiency Nd:$GdVO_4$ laser at 1341nm under 880nm diode laser pumping into the emitting level. *Opt. Commun.* **2009**, *282*, 3565–3567. [CrossRef]
13. Du, C.; Qin, L.; Meng, X.; Xu, G.; Wang, Z.; Xu, X.; Zhu, L.; Xu, B.; Shao, Z. High-power Nd:$GdVO_4$ laser at 1.34 μm end-pumped by laser-diode-array. *Opt. Commun.* **2002**, *212*, 177–181. [CrossRef]
14. Zhang, H.; Liu, J.; Wang, J.; Xu, X.; Jiang, M. Continuous-wave laser performance of Nd:$LuVO_4$ crystal operating at 1.34 μm. *Appl. Opt.* **2005**, *44*, 7439–7441. [CrossRef]
15. Liu, F.; He, J.; Zhang, B.; Xu, J.; Dong, X.; Yang, K.; Xia, H.; Zhang, H. Diode-pumped passively Q-switched Nd:$LuVO_4$ laser at 1.34 μm with a V^{3+}:YAG saturable absorber. *Opt. Express* **2008**, *16*, 11759–11763. [CrossRef]
16. Prado, F.; Franco, T.; Wetter, N. Efficient Trichromatic Nd:YLF Laser Emitting at 1047 nm, 1053 nm and 1314 nm. *Photonics* **2023**, *10*, 1146. [CrossRef]
17. Zhu, H.; Huang, C.; Zhang, G.; Wei, Y.; Huang, L.; Chen, J.; Chen, W.; Chen, Z. High-power CW diode-side-pumped 1341 nm Nd:YAP laser. *Opt. Commun.* **2007**, *270*, 296–300. [CrossRef]
18. Farley, R.; Dao, P. Development of an intracavity-summed multiple-wavelength Nd:YAG laser for a rugged, solid-state sodium lidar system. *Appl. Opt.* **1995**, *34*, 4269–4273. [CrossRef]
19. Son, S.; Song, J.; Kang, J.; Kim, C. Simultaneous second harmonic generation of multiple wavelength laser outputs for medical sensing. *Sensors* **2011**, *11*, 6125–6130. [CrossRef]
20. Weigl, F. A generalized technique of two-wavelength, nondiffuse holographic interferometry. *Appl. Opt.* **1971**, *10*, 187–192. [CrossRef]
21. Abdelsalam, D.; Magnusson, R.; Kim, D. Single-shot, dual-wavelength digital holography based on polarizing separation. *Appl. Opt.* **2011**, *50*, 3360–3368. [CrossRef] [PubMed]
22. Basov, N.; Gubin, M.; Nikitin, V.; Nikuchin, A.; Petrovskii, V.; Protsenko, E.; Tyurikov, D. Highly-sensitive method of narrow spectral-line separations, based on the detection of frequency resonances of a 2-mode gas-laser with non-linear absorption. *Izv. Akad. Nauk. SSR Seriya Fiz.* **1982**, *46*, 1573–1583.
23. Zhang, S.; Tan, Y.; Li, Y. Orthogonally polarized dual frequency lasers and applications in self-sensing metrology. *Meas. Sci. Technol.* **2010**, *21*, 054016. [CrossRef]
24. Huang, H.; Xia, J.; Anh, N.; Li, Y.; Zhang, Y.; Zhang, Q.; Zhao, Z.; Lü, Y. Orthogonally Polarized Dual-Wavelength Pr:LLF Green Laser at 546 nm and 550 nmwith the Balanced Output Powers at All Pump Power Level. *Photonics* **2025**, *12*, 393. [CrossRef]
25. Huang, H.; Xia, J.; Anh, N.; Li, Y.; Lü, Y. Dual-Wavelength Operation at 607 nm and 640 nm with the Same Threshold and Slope Efficiency in Pr^{3+}:$LiLuF_4$ Crystal. *Photonics* **2025**, *12*, 447. [CrossRef]
26. Du, Z.; Hu, Z.; Li, Y.; Anh, N.; Fu, X.; Li, B.; Bai, J. Tunable Yb:GdCOB self-frequency-doubling cyan laser. *Laser Phys. Lett.* **2024**, *21*, 025001. [CrossRef]
27. Zhao, P.; Ragam, S.; Ding, Y.; Zotova, I. Power scalability and frequency agility of compact terahertz source based on frequency mixing from solid-state lasers. *Appl. Phys. Lett.* **2011**, *98*, 131106. [CrossRef]
28. Huang, H.; Li, Y.; Lü, Y.; Anh, N.; Zhang, Q.; Xia, J. Orthogonally Polarized Green Dual-Wavelength Pr^{3+}:$LiLuF_4$ Laser at 523 and 538 nm with the Power Ratio of 1:1. *Photonics* **2025**, *12*, 591. [CrossRef]
29. Junttila, S.; Vastaranta, M.; Liang, X.; Kaartinen, H.; Kukko, A.; Kaasalainen, S.; Holopainen, M.; Hyyppä, H.; Hyyppä, J. Measuring Leaf Water Content with Dual-Wavelength Intensity Data from Terrestrial Laser Scanners. *Remote Sens.* **2017**, *9*, 8. [CrossRef]
30. Najm, M.; Nizamani, B.; Al-Azzawi, A.; Hmood, J.; Abdullah, M.; Harun, S. Generation of dual-wavelength Q-switched laser pulses by employing Mo2Ti2AlC3 MAX phase film. *Opt. Fiber Technol.* **2023**, *81*, 103566. [CrossRef]

31. Chen, M.; Wang, Z.; Zhang, S.; Yang, F.; Zhang, F.; Yuan, L.; He, M.; Li, J.; Zhang, X.; Zong, N.; et al. 1319 nm and 1356 nm dual-wavelength operation of diode-side-pumped Nd:YAG laser. *Opt. Laser Technol.* **2016**, *79*, 52–54. [CrossRef]
32. Guo, L.; Lan, R.; Liu, H.; Yu, H.; Zhang, H.; Wang, J.; Hu, D.; Zhuang, S.; Chen, L.; Zhao, Y.; et al. 1319 nm and 1338 nm dual-wavelength operation of LD end-pumped Nd:YAG ceramic laser. *Opt. Express* **2010**, *18*, 9098–9106. [CrossRef]
33. Lü, Y.; Xia, J.; Zhang, J.; Fu, X.; Liu, H. Orthogonally polarized dual-wavelength Nd:$YAlO_3$ laser at 1341 and 1339 nm and sum-frequency mixing for an emission at 670 nm. *Appl. Opt.* **2014**, *53*, 5141–5146. [CrossRef]
34. Tu, Z.; Dai, S.; Zhu, S.; Yin, H.; Li, Z.; Ji, E.; Chen, Z. Efficient high-power orthogonally-polarized dual-wavelength Nd:YLF laser at 1314 and 1321 nm. *Opt. Express* **2019**, *27*, 32949–32957. [CrossRef]
35. Li, S.; Li, T.; Zhao, S.; Li, G.; Hang, Y.; Zhang, P. 1.31 and 1.32 μm dual-wavelength Nd:$LuLiF_4$ laser. *Opt. Laser Technol.* **2016**, *81*, 14–17. [CrossRef]
36. Badr, T.; Plimmer, M.; Juncar, P.; Himbert, M. Observation by two-photon laser spectroscopy of the $4d^{10}5s^2S_{1/2} \rightarrow 4d_9 5s^{22}D_{5/2}$ clock transition in atomic silver. *Phys. Rev. A* **2006**, *74*, 062509. [CrossRef]
37. Orringer, J.; Kang, S.; Maier, L.; Johnson, T.; Sachs, D.; Karimipour, D.; Helfrich, Y.; Hamilton, T.; Voorhees, J. A randomized, controlled, split-face clinical trial of 1320-nm Nd:YAG laser therapy in the treatment of acne vulgaris. *J. Am. Acad. Dermatol.* **2007**, *56*, 432–438. [CrossRef] [PubMed]
38. Louyer, Y.; Balembois, F.; Plimmer, M.; Badr, T.; Georges, P.; Juncar, P.; Himbert, M. Efficient cw operation of diode-pumped Nd:YLF lasers at 1312.0 and 1322.6 nm for a silver atom optical clock. *Opt. Commun.* **2003**, *217*, 357–362. [CrossRef]
39. Pollak, T.; Wing, W.; Grasso, R.; Chicklis, E.; Jenssen, H. CW Laser Operation of Nd:YLF. *IEEE J. Quantum Electron.* **1982**, *18*, 159–163. [CrossRef]
40. Xu, S.; Gao, S. A new wavelength laser at 1370 nm generated by Nd:YLF crystal. *Mater. Lett.* **2016**, *183*, 451–453. [CrossRef]
41. Shang, P.; Bai, L.; Wang, S.; Cai, D.; Li, B. Research progress on thermal effect of LD pumped solid state laser. *Opt. Laser Technol.* **2023**, *157*, 108640. [CrossRef]
42. Chuang, T.; Verdún, H. Energy Transfer Up-Conversion and Excited State Absorption of Laser Radiation in Nd:YLF Laser Crystals. *IEEE J. Quantum Electron.* **1996**, *32*, 79–91. [CrossRef]
43. Zhang, Z.; Liu, Q.; Nie, M.; Ji, E.; Gong, M. Experimental and theoretical study of the weak and asymmetrical thermal lens effect of Nd:YLF crystal for π- and σ-polarizations. *Appl. Phys.* **2015**, *120*, 689–696. [CrossRef]
44. Huber, G.; Krühler, W.; Bludau, W.; Danielmeyer, H. Anisotropy in the laser performance of NdP_5O_{14}. *J. Appl. Phys.* **1975**, *46*, 3580–3584. [CrossRef]
45. Wang, X.; Yao, J. Transmitted and tuning characteristics of birefringent filters. *Appl. Opt.* **1992**, *31*, 4505–4508. [CrossRef]
46. Fan, T.; Byer, R. Diode laser-pumped solid-state lasers. *IEEE J. Quantum Electron.* **1988**, *24*, 895. [CrossRef]
47. Chen, Y. cw dual-wavelength operation of a diode-pumped Nd:YVO_4 laser. *Appl. Phys. B* **2000**, *70*, 475–478. [CrossRef]

Disclaimer/Publisher's Note: The statements, opinions and data contained in all publications are solely those of the individual author(s) and contributor(s) and not of MDPI and/or the editor(s). MDPI and/or the editor(s) disclaim responsibility for any injury to people or property resulting from any ideas, methods, instructions or products referred to in the content.